CERN – EUROPEAN ORGANIZATION FOR NUCLEAR RESEARCH

CLIC – Note – 988

EM CHARACTERIZATION OF DAMPING MATERIALS FOR CLIC RF ACCELERATING STRUCTURES

G. De Michele, EPLF, Lausanne, Switzerland – PSI, Villigen, Switzerland
A. Grudiev, CERN, Geneva, Switzerland

Abstract

Electromagnetic (EM) characterization of materials up to high frequencies is a major requirement for the correct modelling of many accelerator components: collimators, kickers, high order modes damping devices for accelerating cavities. Different methods and techniques have been used in the past and a unique setup for all kind of materials and frequencies range does not exist. In this note the details of our measurements setup and the different applied methods are described. This work will focus on the coaxial line setup that can be used in a wide range of frequencies. Reflection and transmission methods will be analyzed and discussed. Measurements of silicon carbide (SiC) CerasicB1, EkasicF and EkasicP will be presented.

CERN-OPEN-2013-029
19/08/2013

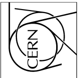

Geneva, Switzerland
19th of August 2013

1. INTRODUCTION

The study of EM properties at microwave frequencies has different fields of applications such as academic research; microwave communications and engineering (military, industrial, civil); clock speeds of electronic devices at microwave frequencies require knowledge of permittivity and permeability; EM interference (EMI) and EM compatibility (EMC). It plays a crucial role in the impedance modeling for the LHC accelerator complex at CERN or for damping materials in CLIC accelerating structures.
Measurement of dielectric properties involves measurements of the complex relative permittivity and complex relative permeability of the materials. A complex dielectric permittivity consists of a real part and an imaginary part. The real part of the complex permittivity, also known as dielectric constant is a measure of the amount of energy from an external electrical field stored in the material. The imaginary part is zero for lossless materials and is also known as loss factor. It is a measure of the amount of energy loss from the material due to an external electric field. The ratio of the imaginary part to the real part of the complex permittivity is called loss tangent. The loss tangent is also called by terms such as tangent loss, dissipation factor or loss factor. The complex permeability also consists of a real part which represents the amount energy from an external magnetic field stored in the material whereas the imaginary part represents the amount of energy dissipated due to the magnetic field. Measurement on the complex permeability is only applicable to magnetic materials. Most materials are non-magnetic and thus, the permeability is very near to the permeability of free space [1].

In the past years different techniques for materials characterization have been developed [2, 3, 4, 5, 6]. We can summarize these techniques in:

- ***Non-resonant techniques***:
  - Reflection method: open-circuited reflection; short-circuited reflection (S_{11})
  - Transmission/reflection methods: (S_{11},S_{12},S_{21},S_{22})

- ***Resonator techniques*** (the sample forms a resonator or a key part of resonator):
  - Dielectric resonator
  - Coaxial surface-wave resonator
  - Split resonator (dielectric sheet sample)

- ***Resonant perturbation techniques***:
  - The sample under test is introduced into the resonator and the EM properties are deduced from the changes in resonance frequency and quality factor of the cavity

- ***Planar circuit techniques*** (both resonant and non-resonant methods):
  - Stripline
  - Microstripe
  - Coplanar line

In a more general view we can split the techniques in two big families: a) non-resonant techniques that give the possibility to measure EM properties in a wide range of frequencies and b) resonator techniques that allow measuring the EM properties at single or several discrete

frequencies and are higher sensitivity and higher accuracy techniques than the non-resonant techniques.
This note presents the non-resonant technique with a coaxial line filled with the material under test (MUT). Both reflection and transmission methods will be investigated and discussed. For the reflection method, the properties of the material are obtained from the measured reflection coefficient by using it as input for a transmission line (TL) model or for 3D EM simulations, which describe the measurement setup. The transmission method will use only the EM simulations in order to infer the EM properties of materials. These methods have been applied to characterize samples of SiC which could be used for LHC collimators and for CLIC accelerating structures.

2. THE COAXIAL TECHNIQUE

A coaxial line has been used in order to characterize the material under test with two different methods: reflection and transmission methods.
For the reflection method the coaxial line is closed on a well-known load. Using a network analyzer the reflection coefficient is measured (see Figure 1) [7].

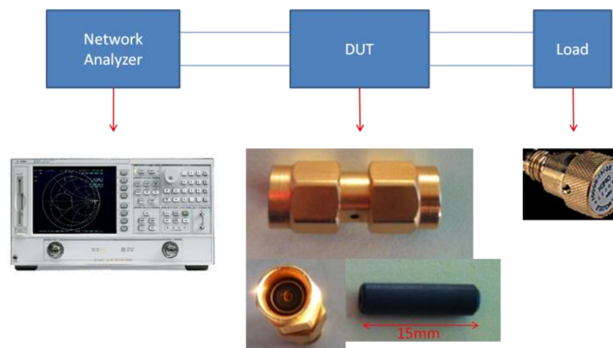

Figure 1: Measurements setup for the reflection method.

The measured parameter is related to the unknown material properties. This function can be obtained numerically (from 3D finite elements simulations) or from TL theory.

a. Study of feasibility of the method

The feasibility of the adopted method was studied using a 3D EM simulator as the environment for ideal measurements and a TL model to obtain the reflection coefficient as function of the material properties. The same function is obtained also numerically from the 3D EM code CST Microwave Studio®. The flowchart of Figure 2 explains these two different procedures.

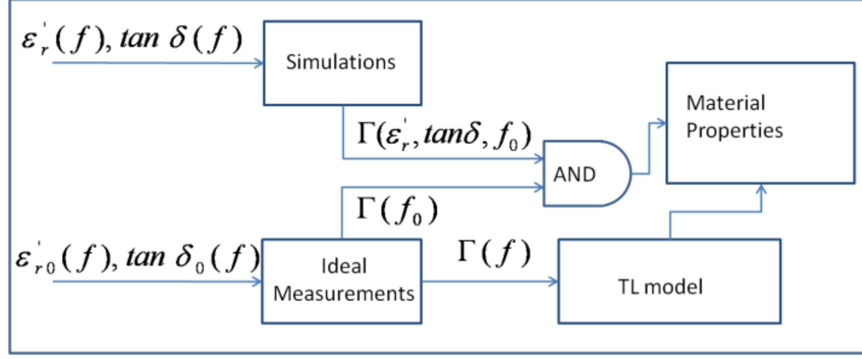

Figure 2: Flowchart for simulations and TL model techniques.

The measurement system is simulated using the material properties (real permittivity and electric loss tangent) as free parameters; the output of the simulations is always the reflection coefficient in a certain range of frequencies. From the simulations we obtain the complex reflection coefficient as a function of real permittivity and loss tangent at a given frequency (see Figure 3). The same function can be obtained also analytically by modelling the measurement system with the transmission line theory where the reflection coefficient can be calculated from the impedance of the input line and the impedance at the section AA' (see Figure 4).

$$\Gamma_{AA'} = \frac{Z_{AA'} - Z_0}{Z_{AA'} + Z_0} \tag{1}$$

where $Z_{AA'}$ can be calculated by the transport of the impedance of the load along the transmission line. For a lossy line it is:

$$Z_{AA'} = Z_{DUT} \frac{Z_{load} + Z_{DUT} \tanh(jk_{DUT} L)}{Z_{DUT} + Z_{load} \tanh(jk_{DUT} L)} \tag{2}$$

where k_{DUT} is the complex propagation constant given by:

$$k_{DUT} = \beta - j\alpha \tag{3}$$

where α is the attenuation constant and β is the phase propagation constant.

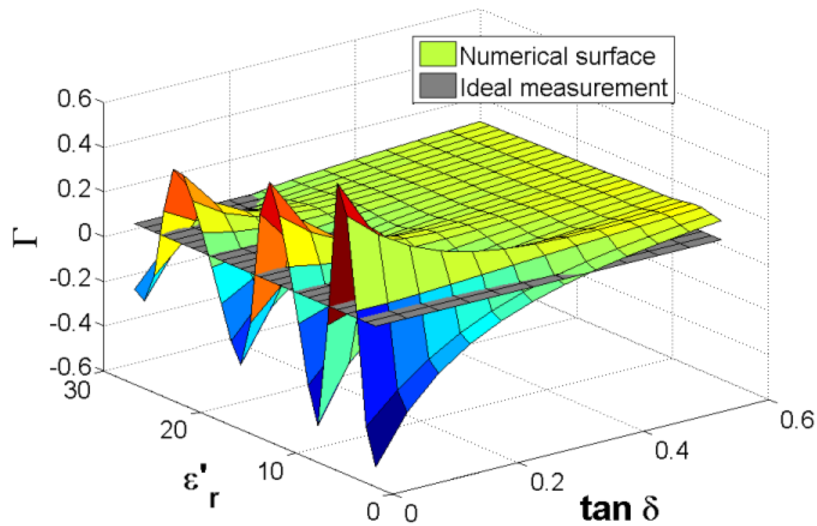

Figure 3: Reflection coefficient as function of loss tangent and real permittivity.

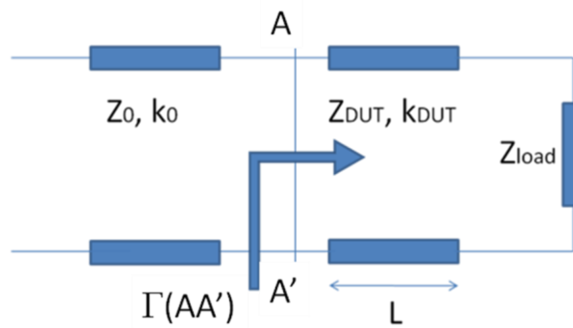

Figure 4: Transmission line model.

By using the function as calculated numerically we found the possible solutions of real permittivity and loss tangent from the contour plot that results from the intersections between the 3D surfaces, obtained numerically, and the ideal measurements i.e. the simulation of the reflection coefficient Γ at one single frequency for given material properties. Figure 3 shows the intersection of one 3D surface with the ideal measurements at a certain frequency.

Figure 5 shows contour plots for different 3D surfaces and points from the TL model. Different contour plots are displayed for different terminations of the transmission line (open circuit and short circuit) and for the real part and the imaginary part of Γ. The solution is the intersection point of all configurations. In this example the solution gives 10 for the real part of the complex permittivity and 0.2 for the loss tangent. These results are confirmed by the TL model and in fact the solutions for the short and the open end lie exactly on the intersection of all contour plots.

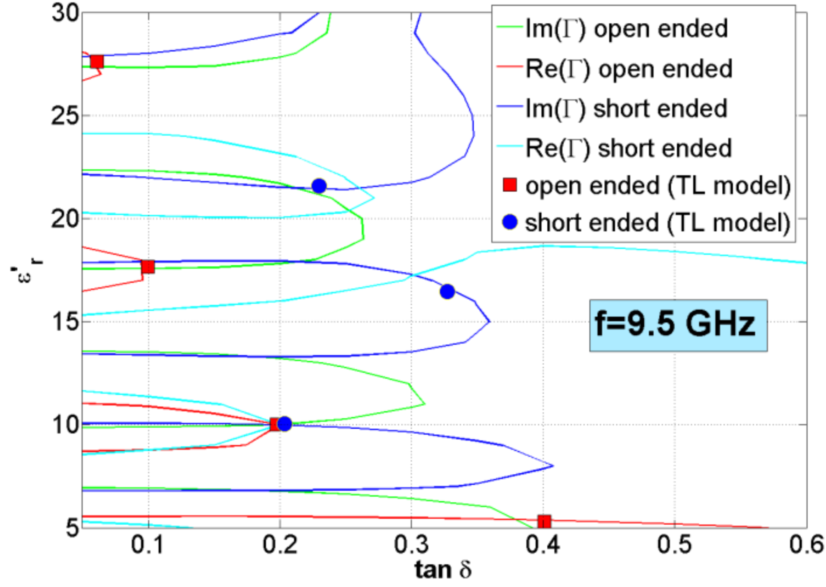

Figure 5: Contour plots for different 3D surfaces. The squared and round dots are calculated from transmission line model.

b. Measurements of dielectric materials: air-gap correction

One complication of the coaxial method is the presence of air-gap in the fabrication process for the sample under test (see Figure 6). A correction to the characteristic impedance can be introduced to take into account the air-gap effect. Due to the air-gap the capacitance and the inductance have the following expressions:

$$C_{sample} = \frac{2\cdot\pi\cdot\varepsilon_0\cdot\varepsilon_r\cdot l}{\ln\left(\frac{d_{sample}}{d_{air}}\right)} \qquad C_{in} = \frac{2\cdot\pi\cdot\varepsilon_0\cdot\varepsilon_r\cdot l}{\ln\left(\frac{d_{air}}{d}\right)} \qquad C_{out} = \frac{2\cdot\pi\cdot\varepsilon_0\cdot\varepsilon_r\cdot l}{\ln\left(\frac{D}{d_{sample}}\right)} \tag{4}$$

$$L_{sample} = \frac{\mu_0\mu_r}{2\cdot\pi}\ln\left(\frac{d_{sample}}{d_{air}}\right)\cdot l \qquad L_{in} = \frac{\mu_0\mu_r}{2\cdot\pi}\ln\left(\frac{d_{air}}{d}\right)\cdot l \qquad L_{out} = \frac{\mu_0\mu_r}{2\cdot\pi}\ln\left(\frac{D}{d_{sample}}\right)\cdot l \tag{5}$$

where:

$$\mu_0 = 4\pi\cdot 10^{-7}\,H/m$$
$$\varepsilon_0 = 8.854\cdot 10^{-12}\,F/m$$

$$\varepsilon_r = \varepsilon' - j\left(\varepsilon'' + \frac{\sigma}{\omega}\right) = \varepsilon'\left(1 - j\tan\delta - j\frac{\sigma}{\omega\varepsilon'}\right) \tag{6}$$

For dielectrics and in our frequency range of interest: $\frac{\sigma}{\omega\varepsilon^{'}} << 1$.

$$\frac{1}{C_{tot}} = \frac{1}{C_{sample}} + \frac{1}{C_{in}} + \frac{1}{C_{out}} \tag{7}$$

$$L_{tot} = L_{sample} + L_{in} + L_{out} \tag{8}$$

$$Z_{DUT} = \sqrt{\frac{L_{tot}}{C_{tot}}} \tag{9}$$

$$k_{DUT} = \frac{\omega}{c}\sqrt{\mu_r \varepsilon_r} - j\frac{1}{\sigma\delta\,(2\pi \cdot Z_{DUT})} \cdot \frac{(D+d)}{D \cdot d} \tag{10}$$

and

$$\delta = \frac{1}{\sqrt{\pi f \mu\sigma}} \text{ is the skin depth} \tag{11}$$

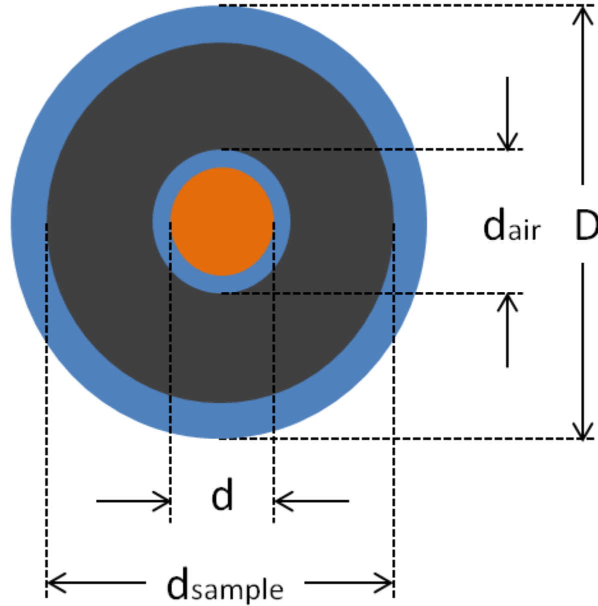

Figure 6: Air-gaps considered in the TL model.

where C_{sample} and L_{sample} are the classical capacitance and inductance of a coaxial cable and C_{in}, C_{out} and L_{in}, L_{out} the additive capacitances and inductances due to the air gaps [8]. Nevertheless our samples were machined with an air gap less than 50um that in the frequency range of interest gave only few percent errors on the final results.

3. THE REFLECTION METHOD

Particularly attention has been done on the choice of the measurements setup: the simulated structure consists of three pieces of coaxial adapters. The piece near the source is a SMA connector filled by the material under test followed by a 3.5mm adapter in air. The coaxial line is terminated by a short circuit or an open circuit.

Two different methods have been investigated: the reflection method and the transmission method. For the reflection method we have used TL model and EM simulations to infer the EM properties (see scheme in Figure 2).

The open and the short are Agilent standards and have been modeled by introducing the constructor fringe capacitance and the residual inductance (see Figure 7):

$$C = C_0 + C_1 \cdot f + C_2 \cdot f^2 + C_3 \cdot f^3 \tag{12}$$

$$L = L_0 + L_1 \cdot f + L_2 \cdot f^2 + L_3 \cdot f^3 \tag{13}$$

The impedance of the standards is:

$$Z_S = Z_0 \frac{Z_{C/L} + jZ_0 \tan(k_S l_S)}{Z_0 + Z_{C/L}\, j \tan(k_S l_S)} \tag{14}$$

where $Z_C = \frac{1}{j\omega C}$ and $Z_L = j\omega L$.

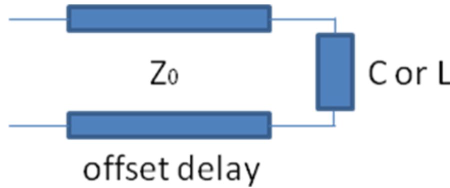

Figure 7: TL model for open and short standards.

A sensitivity study has shown that a variation of the length of open and short within ±1% implies ±9‰ on the permittivity and a variation of the length of open and short of +10% implies -9% on the permittivity. Furthermore ±50% on pairs (C0, L0), (C1, L1), (C2, L2), (C3, L3) gives respectively Δepsr'=1‰, 1‰, <1‰, <<1‰. The capacitance of the open circuit accounts for strong variation of the real part of permittivity. The inductance of the short circuit accounts for a very little variation on real part of permittivity. With no-inductance at all there is a Δepsr'=1‰.

The used EM code is HFSS [9]. A comparison between the TL model, HFSS simulation and measurements have been done for a setup assembled with the DUT (air), a 3.5 mm adapter and the load that in this case (reflection method) is either a short circuit or an open circuit (see Figure 8). The choice of using a 3.5 mm adapter came from the necessity to use the same standard (short or open) both in the calibration of the network analyzer and in the measurements of EM material properties. The pictures in Figure 9 show the whole assembly.

The reflection coefficient is calculated similarly to the expression (2) at each different section of the DUT. The characteristic impedance of the coaxial line in air is:

$$Z_{AIR} = 60\sqrt{\frac{\mu_r}{\varepsilon_r}}\ln\left(\frac{d_{out}}{d_{in}}\right) \tag{15}$$

where d_{out} and d_{in} are the outer and the inner diameter of each section. Considering losses in the conductors, the complex propagation constant is:

$$k_{AIR} = \frac{\omega}{c}\sqrt{\mu_r\varepsilon_r} - j\frac{1}{\sigma\delta(2\pi \cdot Z_{AIR})}\cdot\frac{(d_{out}+d_{in})}{d_{out}\cdot d_{in}} \tag{16}$$

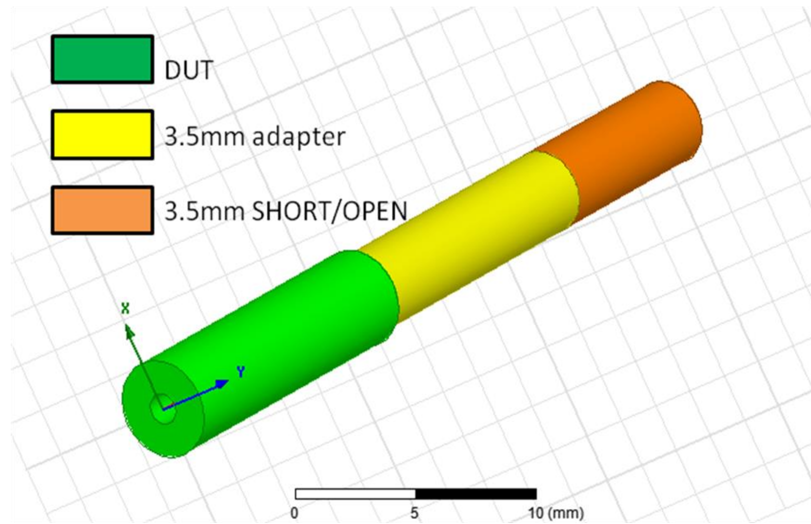

Figure 8: HFSS simulated geometry.

Figure 9: Measurements with reflection method.

In order to reduce the errors from different pieces of the DUT a separated study has been done on the different parts. First the short and the open standards have been measured (S_{11} in module and

phase) and compared to the TL model. The geometric characteristics of the short/open standards are:

- Dout = 3.50mm
- Din = 1.52mm
- Short/Open length = 9.53mm/9.49mm

The length of the MUT is such that in the frequency range of interest the EM wave is attenuated but still measurable by the network analyzer; in fact the attenuation of the wave while passing through the material at the highest frequency (27GHz) goes according to:

$$e^{-j\gamma 2L} = e^{-j\frac{2\pi}{\lambda_0}\sqrt{\varepsilon_r^{'}}\sqrt{1-j\frac{\varepsilon_r^{''}}{\varepsilon_r^{'}}}\cdot 2L} \tag{17}$$

In the hypothesis that $\varepsilon_r^{''} << \varepsilon_r^{'}$ this yields:

$$e^{-j\gamma 2L} \approx e^{-j\frac{2\pi}{\lambda_0}\sqrt{\varepsilon_r^{'}}\left(1-j\frac{\tan\delta}{2}\right)\cdot 2L} = e^{-j\frac{2\pi}{\lambda_0}\sqrt{\varepsilon_r^{'}}\cdot 2L}\cdot e^{-\frac{\pi}{\lambda_0}\sqrt{\varepsilon_r^{'}}\tan\delta\cdot 2L} \tag{18}$$

and taking the value of the envelope one has e.g. for CerasicB1 at 27GHz, roughly -40dB.
Figure 10 shows the measurements of the scattering parameter S_{11} and the TL model for the standards. The error of the measurements with respect to the TL model is less than one per mille. The fringe capacitance and the residual inductance did not influence the results.

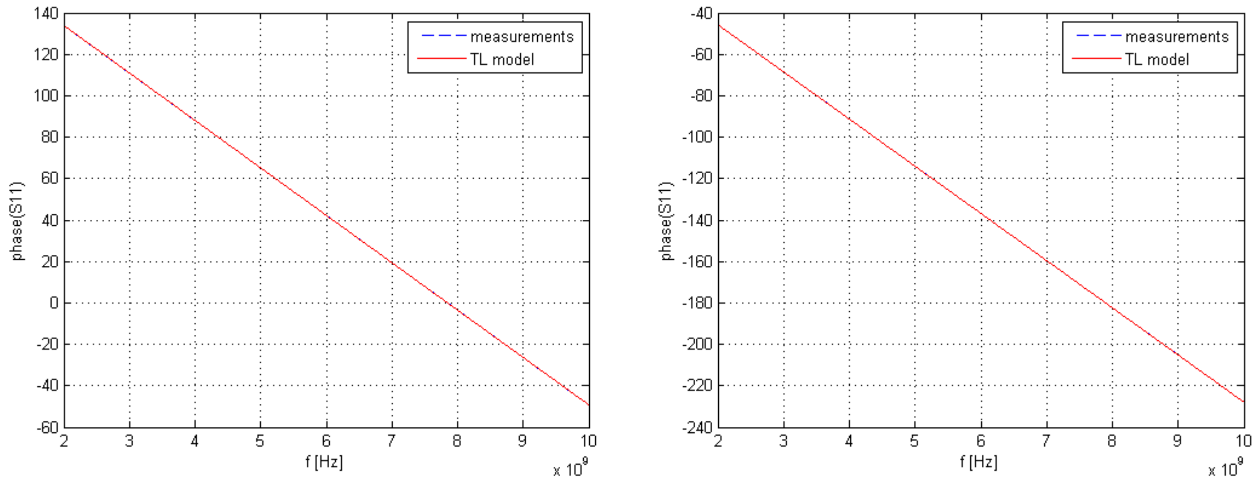

Figure 10: phase of S_{11} for open and short standards.

Once verified that the standards could be well simulated, the SMA adapter (air) and the 3.5mm adapter have been introduced in the calculations. Now the simulated line is that shown in Figure 8 and the simulations take into account also the losses in the conductors.
The length of the SMA adapter is fixed to 15.00mm and an optimization procedure was launched by varying the following parameters:

– Outer and inner diameter of SMA
– Outer and inner diameter of 3.5mm adapter
– Length of 3.5mm adapter
– Conductivity of materials

Table 1 shows the initial values before and after optimization with TL model.

Table 1: Optimization procedure for short circuit configuration.

	D [mm]	**D [mm]**	**Dout [mm]**	**Din [mm]**	**Sigma [S/m]**	**L_3.5mm [mm]**
Before	4.12	1.30	3.50	1.52	5.8e7	--
After (real(S11))	4.18 (1.4%)	1.26 (-3%)	3.48 (-0.6%)	1.50 (-1.3%)	5.8e7 (0%)	15.6 (--)
After (imag(S11))	4.18 (1.4%)	1.26 (-3%)	3.48 (-0.6%)	1.50 (-1.3%)	5.8e7 (0%)	15.6 (--)

Figure 11 and Figure 12 show the real and imaginary part of the scattering parameter S_{11} for the studied geometry (short circuit configuration and open circuit configuration) by comparing the measurements (blu line) and the TL model (red line).

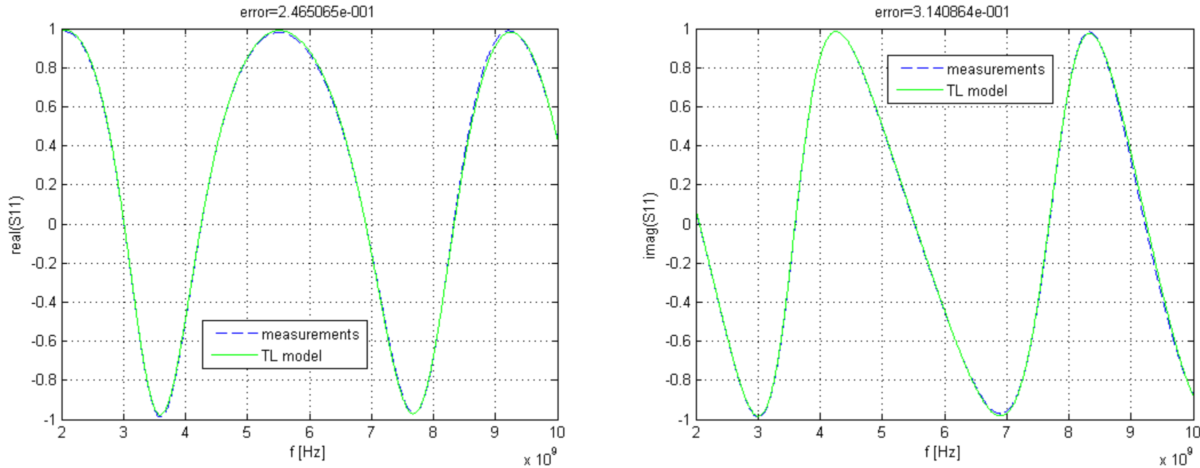

Figure 11: real(S_{11}) and imag(S_{11}) for the TL in Figure 8. The MUT is air. The configuration is short ended.

Table 2: Optimization procedure for open circuit configuration.

	D [mm]	**d [mm]**	**Dout [mm]**	**Din [mm]**	**Sigma [S/m]**	**L_3.5mm [mm]**	**C0**	**C1**	**C2**
Before	4.12	1.30	3.50	1.52	5.8e7	--	494e-16	-310e-27	23.2e-36
After (real(S11))	4.18 (1.4%)	1.26 (-3%)	3.48 (-0.6%)	1.50 (-1.3%)	5.8e7 (0%)	15.6 (--)	0.5e-16	-50e-27	6e-36
After (imag(S11))	4.18 (1.4%)	1.26 (-3%)	3.48 (-0.6%)	1.50 (-1.3%)	5.8e7 (0%)	15.6 (--)	0.5e-16	-50e-27	6e-36

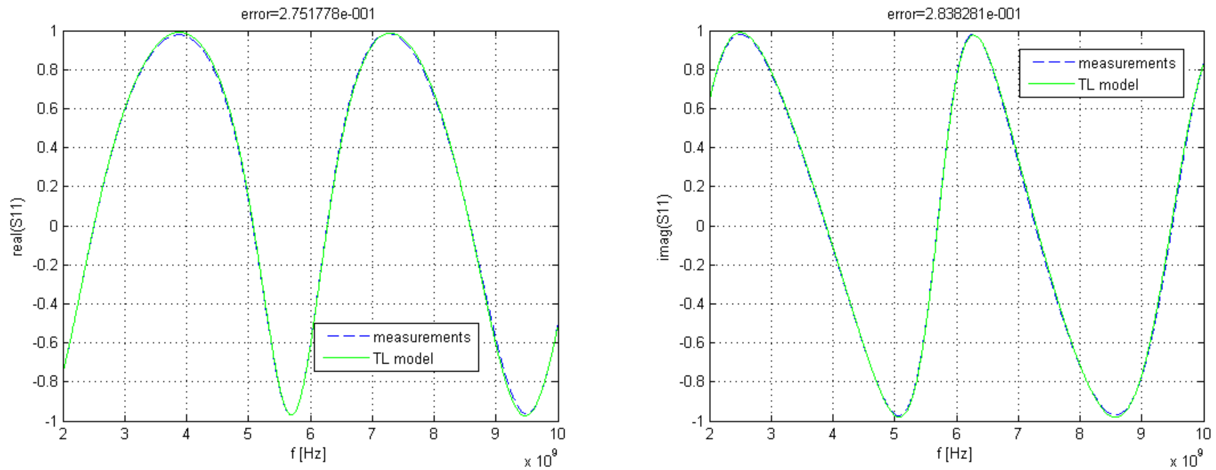

Figure 12: real(S_{11}) and imag(S_{11}) for the TL in Figure 8. The MUT is air. The configuration is open ended.

Furthermore we compared the measurements with HFSS simulations before and after optimization for short and open circuit configurations.

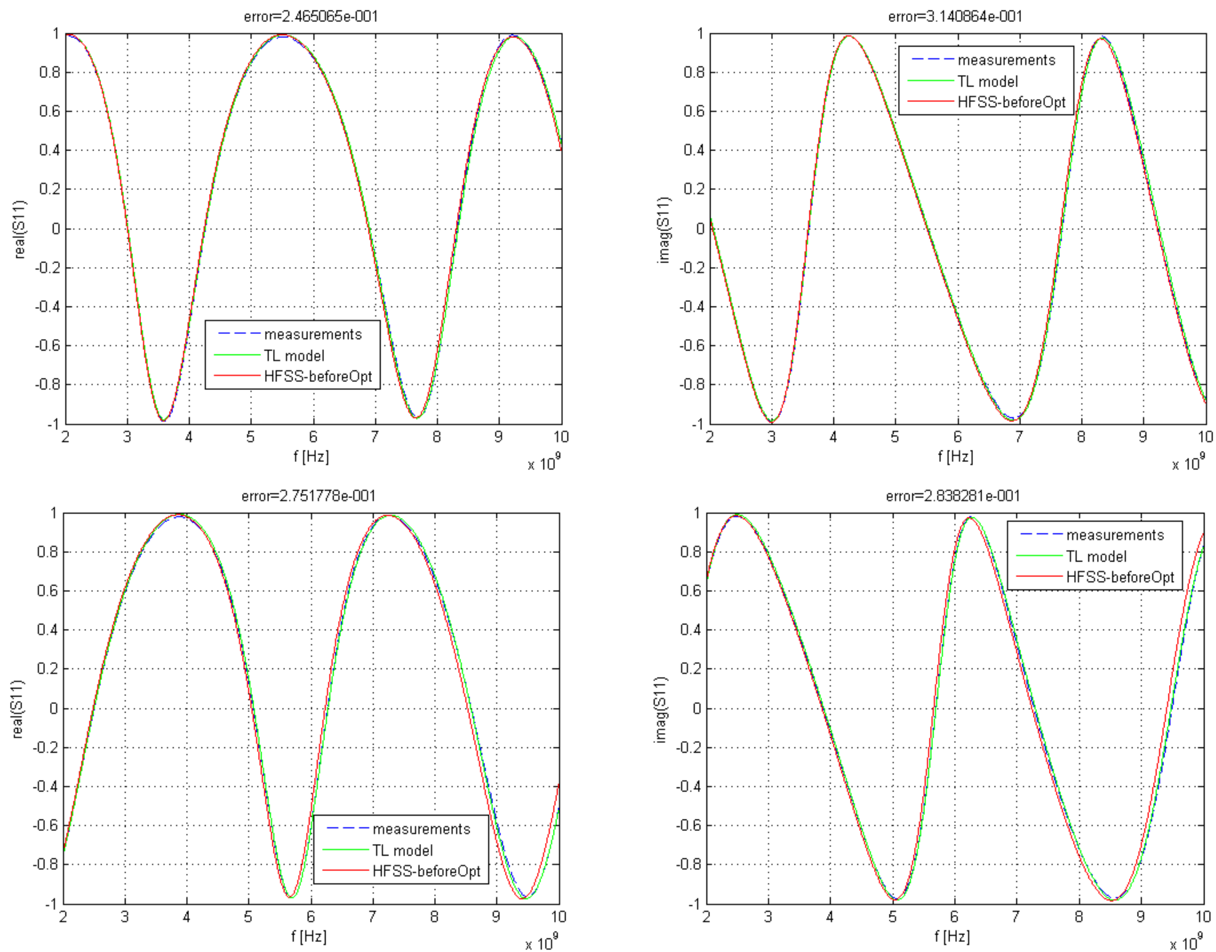

Figure 13: comparison among measurements, TL model and HFSS before optimization.

Figure 13 shows that there is a shift in frequency of the complex S_{11} with respect to the measurements for the open ended configuration. This shift is due to the different cross section of the SMA and the 3.5mm adapters. In order to take into account the variation of the transverse sections, the length of the open standard should be reduced to 9.22mm. The length of the short is now 9.43mm. The optimization process in HFSS has been carried on by varying the length of the 3.5mm and the SMA adapters: a length of 15.25mm (for both short/open configurations) for the 3.5mm adapter and a length of 15.15mm for the SMA adapter were considered. Figure 14 shows the results.
The method of the least squares between the S_{11} of the TL model and the measured one has been applied to calculate the errors (see **Table 3** and **Table 4**).

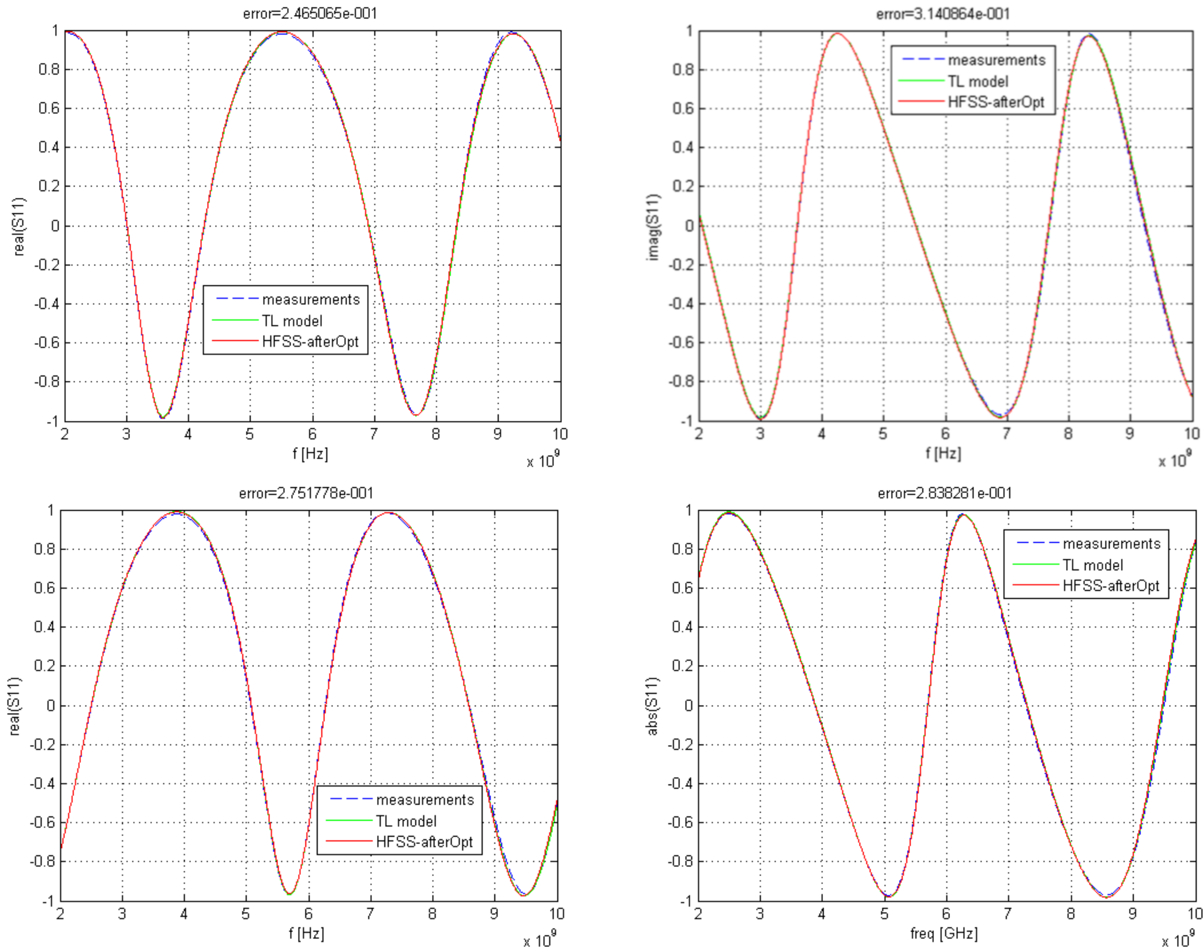

Figure 14: comparison among measurements, TL model and HFSS after optimization.

Table 3: comparison of errors for the scattering parameter S_{11} for TL model and HFSS with respect to measurements

	Meas. vs. TL model	**Meas. vs. HFSS**
Real(S11) for SC	0.246	0.212
Imag(S11) for SC	0.314	0.224
Real(S11) for OC	0.275	0.356
Imag(S11) for OC	0.284	0.472

In the TL model the 3.5mm adapter was 15.60 mm long and the SMA adapter 15.00 mm long. By keeping the same lengths ratio of the HFSS simulation (15.25/15.15), the TL model had 15.35 mm long 3.5mm adapter and 15.25mm long SMA adapter. The results are in Figure 15. In Table 3 are resumed the errors of the TL model and HFSS simulations with respect to the measurements.

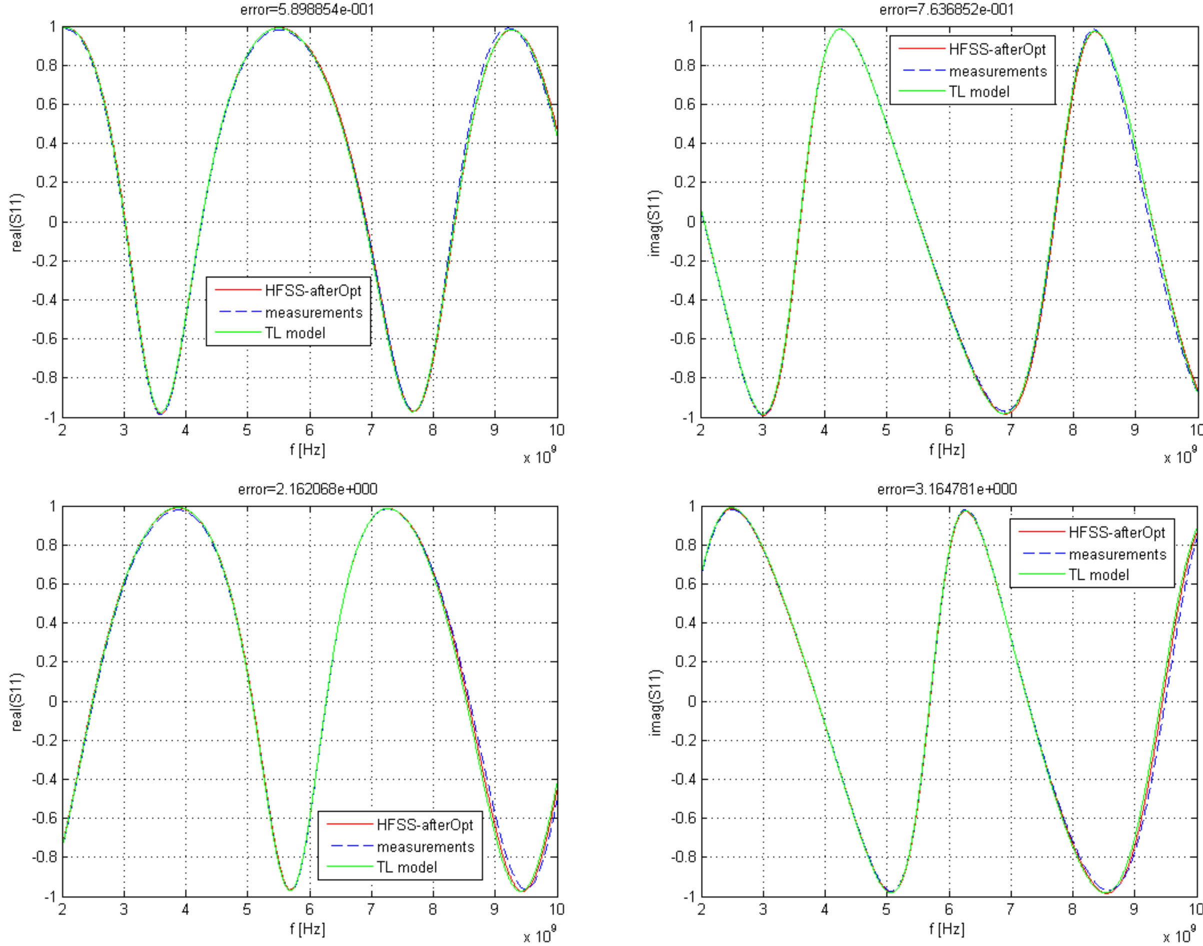

Figure 15: comparison among measurements, TL model and HFSS after optimization.

Table 4: comparison of errors for the scattering parameter S11 for TL model, HFSS and measurements

	Meas. vs. TL model	**Meas. vs. HFSS**	**TL model vs. HFSS**
Real(S11) for SC	0.590	0.819	0.196
Imag(S11) for SC	0.764	0.968	0.198
Real(S11) for OC	2.162	0.799	0.329
Imag(S11) for OC	3.165	1.097	0.411

Until now the DUT was filled with air. The next step was the introduction of the dielectric. To check the consistency of the TL model and HFSS, different simulations in HFSS with the same geometry of TL model have been performed:

a) With losses in conductors and w/o losses in dielectric
b) W/o losses in dielectric and w/o losses in conductors

c) With losses in dielectric and w/o losses in conductors

An ideal material with a real part of relative permittivity equal to 13.5 and the imaginary part equal to 1.2 in the frequency range from 2 to 10GHz was considered.
Figure 16 shows the results for the short circuit configuration. This analysis shows the consistency of losses in TL model and HFSS (same value of amplitudes) but no consistency between the TL model and HFSS with respect to the length of the line. This is the reason why in HFSS the line should be shorter in order to compensate the additional length in the 3D model in presence of different cross sections.

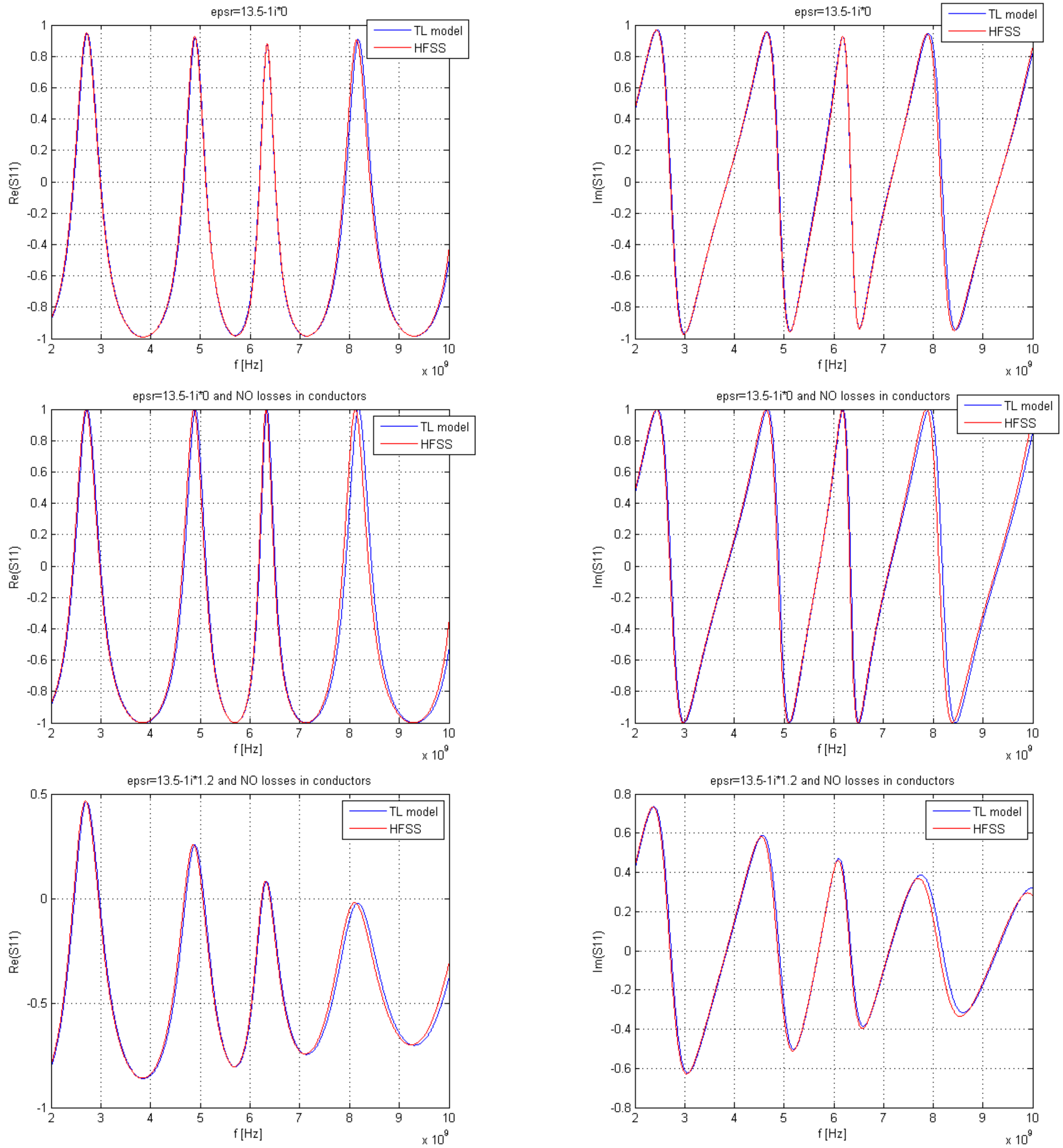

Figure 16: S_{11} for short circuit configuration for a) loss in conductors and no losses in dielectric b) no losses both in conductors and dielectric c) losses in dielectric and no losses in conductors.

As said before if in HFSS the line is shorter, for instance 15.25mm for 3.5mm and 15.15 for SMA whilst in TL model one has 15.25mm for both 3.5mm and SMA, the S_{11} matches for both cases. In TL model in order to fit S_{11}, we have 15.25mm for both 3.5mm and SMA.

Figure 17 shows the perfect matching between simulations and TL model with losses in materials and in conductors. The material had epsr=13-i3 constant in all frequency range.

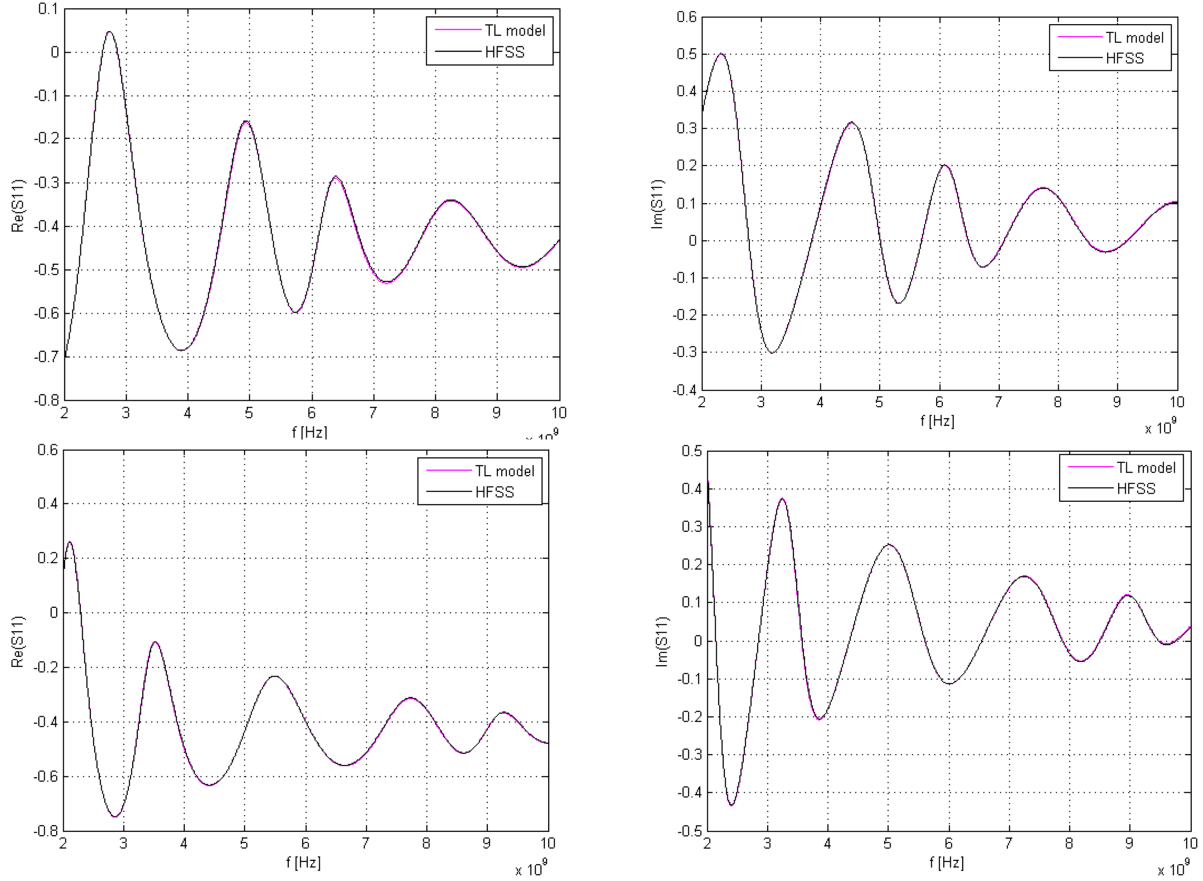

Figure 17: Real(S_{11}) and Imag(S_{11}) for a generic material with losses in material and conductors. Top plots for short circuit and bottom for open circuit.

a. Losses

In the TL model all kind of losses have been included in the calculations. In general, the losses for a transmission line are:

- Losses due to metal conductivity α_c: in a TL this kind of loss is modeled by a series resistance per unit length and is function of TL geometry and RF surface resistance of the used metal. For a coaxial line the expression is:

$$\alpha_c = \frac{R_m}{2\pi \cdot Z_C} \cdot \frac{(d_{out} + d_{in})}{d_{out} \cdot d_{in}} \tag{19}$$

Where Z_C is the characteristic impedance of the coaxial line, d_{out} the outer diameter, d_{in} the inner diameter, R_m is the real part of the surface impedance of the TL with finite conductivity. The expression for the surface impedance is:

$$Z_m = \frac{1+j}{\delta \cdot \sigma} \qquad (20)$$

- Losses due to dielectric loss tangent α_d : very important at microwave frequencies because is proportional to the frequency, so the higher the frequency, the more likely it will dominate overall loss (metal loss is only proportional to square root of frequency). For a coaxial line the expression is:

$$\alpha_d = \frac{\omega}{c} \frac{\varepsilon^{''}}{2\sqrt{\varepsilon_r^{'}}} \qquad (21)$$

- Losses due to conductivity of dielectric α_G : the loss due to substrate conductivity is often ignored because it is usually very small because the dielectric has extremely low conductivity. With the use of silicon (semiconductor) in microwave engineering this attenuation is very important. This kind of loss is neither a function of frequency nor of geometry but only function of conductivity and dielectric constant.

- Losses due to radiation α_R : zero for our coaxial setup.

b. Check of the routine for the extraction of the EM properties

The TL model for the extraction of the EM properties of materials has been checked by using as input the S_{11} generated by the TL model itself by considering a material with relative permittivity epsr=13-i3. This procedure is equivalent to consider an ideal measurement. Figure 18 shows the output of the routine (i.e. the real and imag part of epsr) for the considered input. The results match perfectly with the expectation.

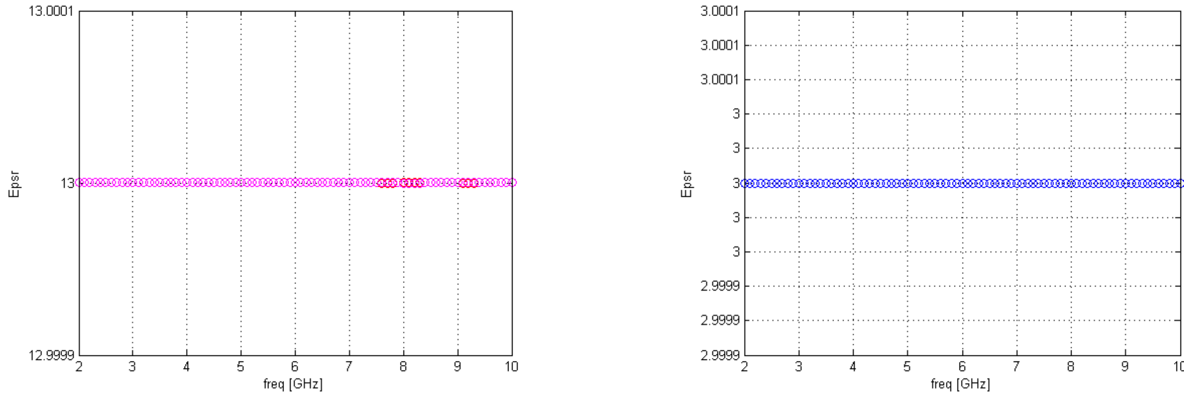

Figure 18: S_{11} calculated with TL model for an input given by a material of epsr=13-i3

The same check of the routine was done by using HFSS simulations. Also in this case we used as ideal measurement the scattering parameter S_{11} calculated from a simulation with a material properties equal to epsr=13-i3.

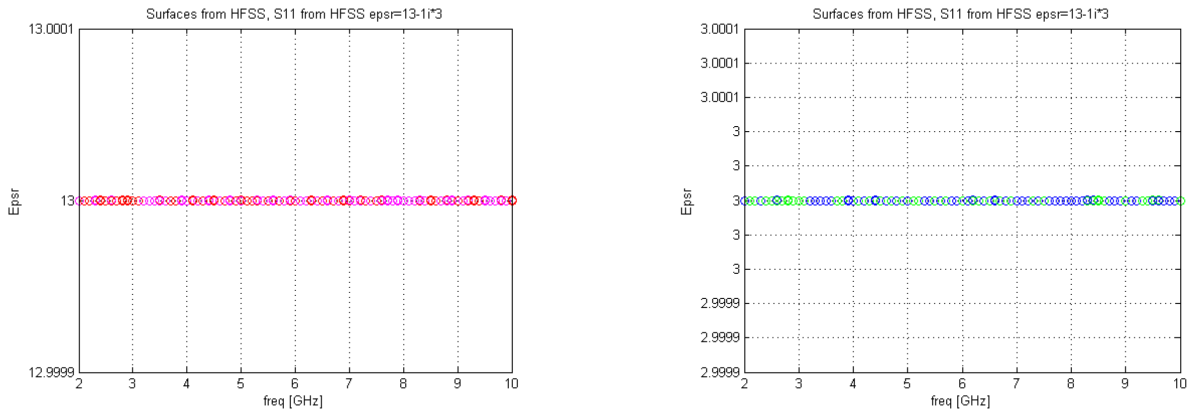

Figure 19: S_{11} calculated with HFSS simulations for an input given by a material of epsr=13-i3

c. Measurements with the reflection method

After crosscheck the HFSS simulations and the TL model we measured the properties of EkasicF, EkasicP in 2-10GHz frequency range.

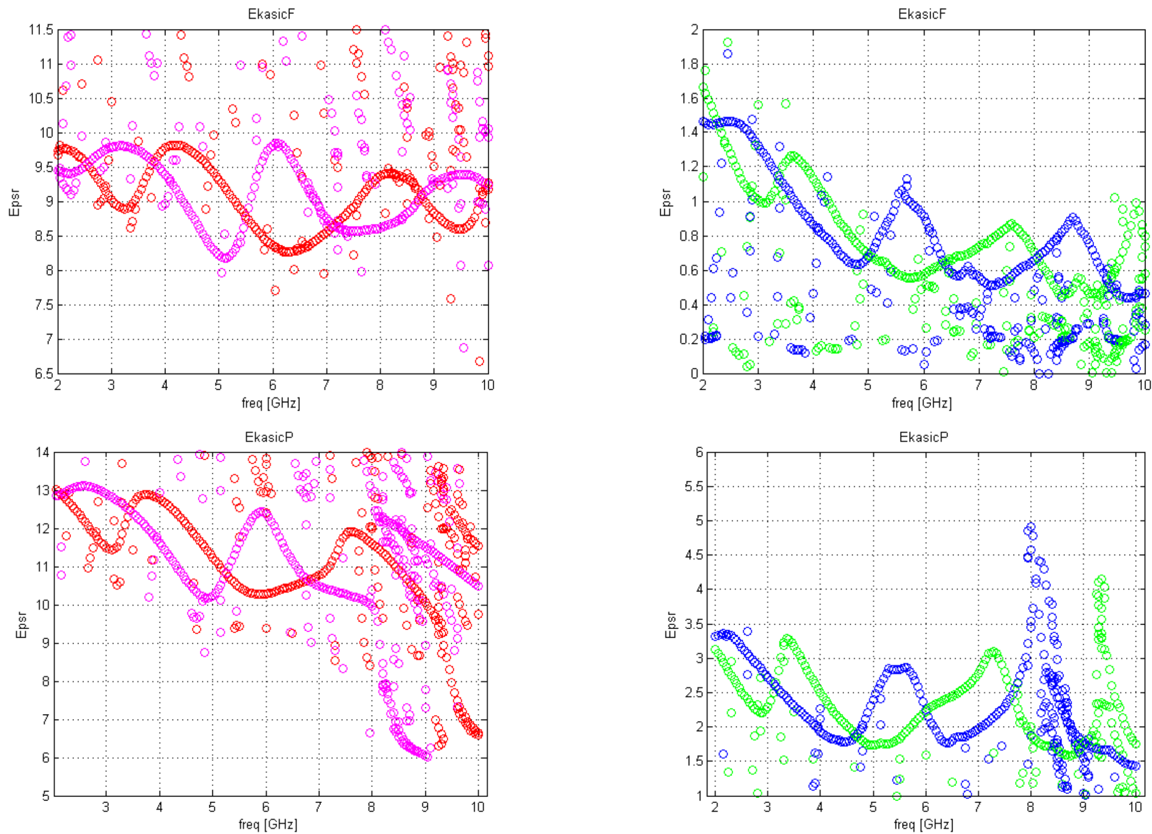

Figure 20: Measurements of complex permittivity for EkasicF and EkasicP in the frequency range 2-10 GHz. HFSS has been used to calculate the dependence of the reflection coefficient on the

real and imaginary parts of permittivity.

Figure 20 shows the EM properties by using the HFSS simulations and Figure 21 by using the TL model for calculating the dependence of the reflection coefficient on the real and imaginary parts of permittivity.

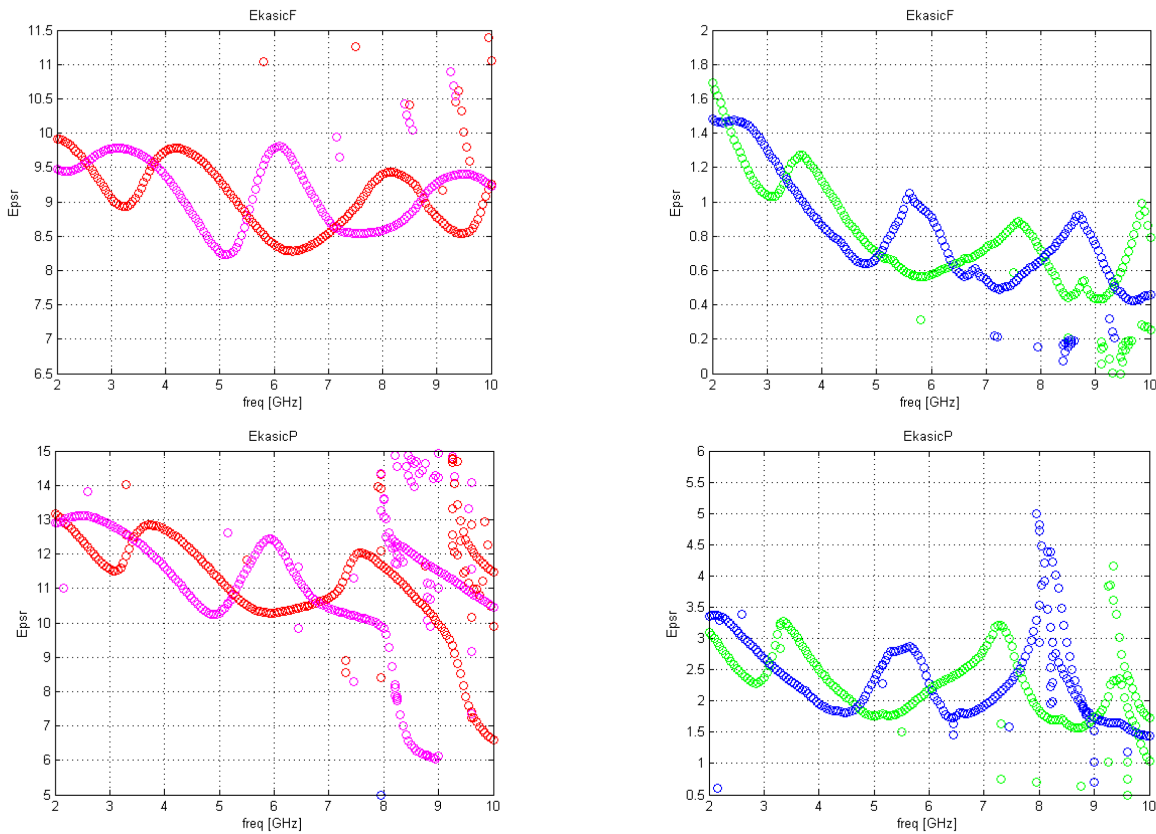

Figure 21: Measurements of complex permittivity for EkasicF and EkasicP in the frequency range 2-10GHz. The TL model has been used to calculate the dependence of the reflection coefficient on the real and imaginary parts of permittivity.

As said before the solution is the intersection of the curves for the short and open circuit. Since there are only few points of intersection, the average solution is shown for EkasicF and EkasicP in **Figure 22**.

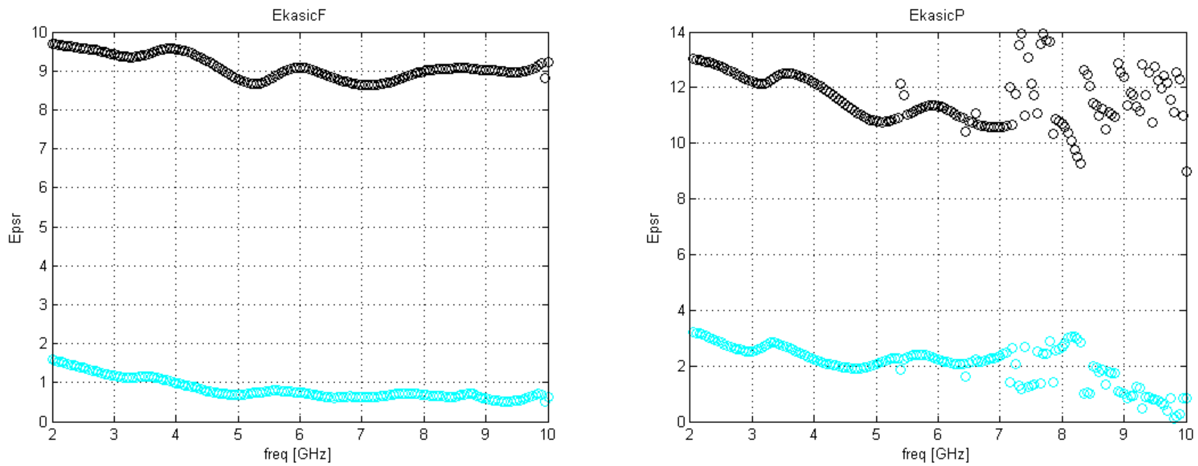

Figure 22: average solution of the short and open circuit configurations for EkasicF and EkasicP in the frequency range 2-10GHz.

This analysis shows that with this setup the EM properties can be found up to 10GHz for EkasicF and up to 7GHz for EkasicP. Furthermore lossier is the material more difficult is the characterization at higher frequencies.

4. THE TRANSMISSION METHOD

The reflection method gave some limitations on the maximum measurable frequency range. For this reason transmission method has been evaluated.

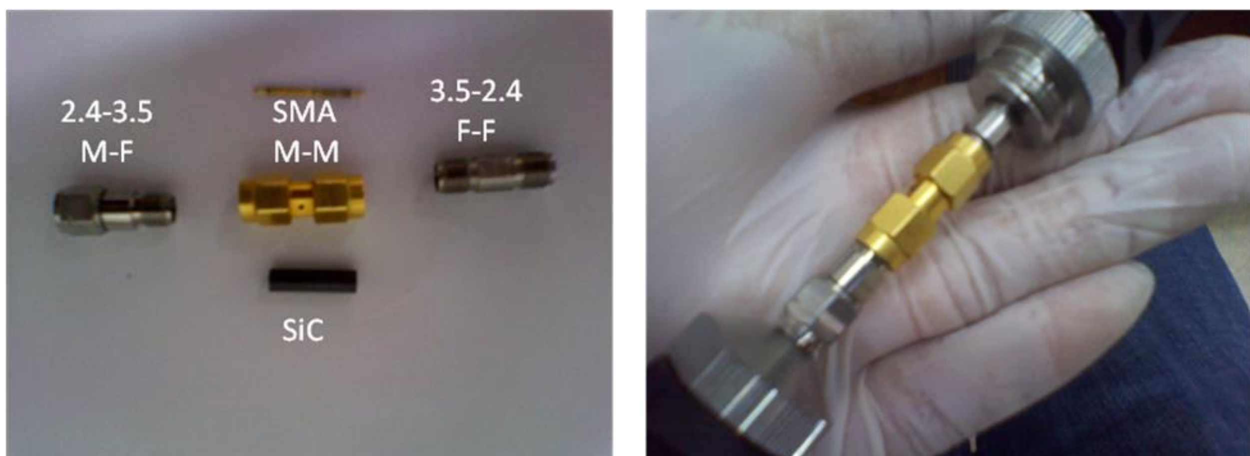

Figure 23: Measurements with the transmission method.

The setup consists on a SMA adapter filled by the material with a hollow coaxial shape (see Figure 23). The dimensions of the samples are:

- Length = 15.00±0.02mm
- Outer diameter = 4.07±0.01mm
- Inner diameter = 1.30±0.02mm

The hollow coaxial shape samples were measured in two frequency range: from 2GHz to 10GHz and from 10GHz to 27GHz. The reason for these two ranges was to improve the calibration of the network analyzer. The calibrated planes are directly the 3.5mm connectors. This is important in order to reduce any error due to possible transitions between the connector-adapter-DUT.
Figure 24 shows the measured scattering parameter S_{21} for CerasicB1, EkasicF and EkasicP. Often such extrapolation gives more than one solution. The right solution is easily extracted by continuity of the value of the parameter (real or imag epsr). One could apply a filter in order to clean for the non-solutions. The results of the EM properties are plotted in Figure 25.

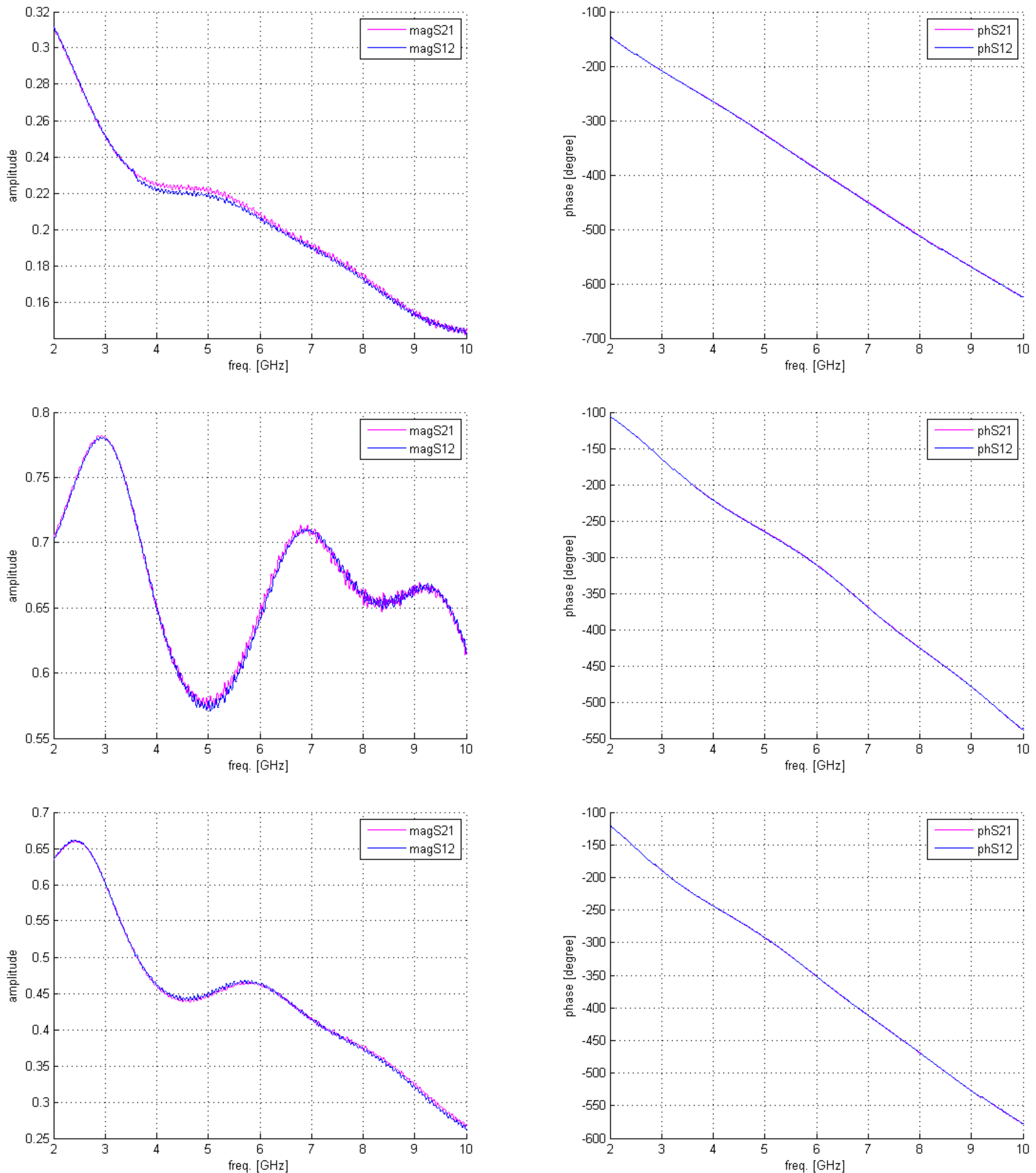

Figure 24: Measured scattering parameters in amplitude and phase. Top: CerasicB1; Middle: EkasicF; Bottom EkasicP.

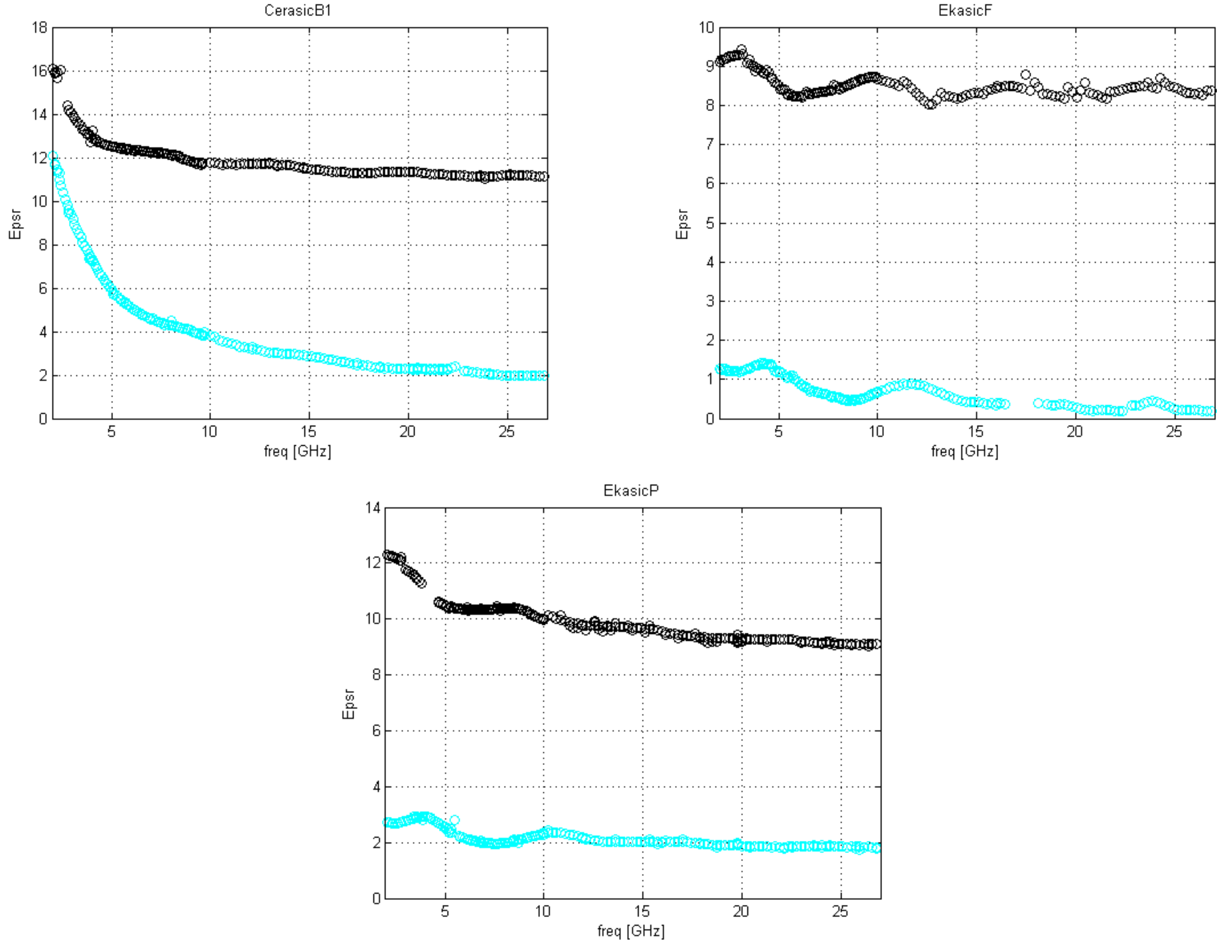

Figure 25: Relative permittivity for CerasicB1, EkasicF and EkasicP measured with the transmission method. The black curve refers to the real part and the blue light curve refers to the imaginary part of the relative permittivity.

Figure 26 shows the fit of the measurements with the Cole-Cole Model that presents the same characteristics of a low-pass filter with simple poles. The analytical expression yields:

$$\varepsilon_r(\omega) = \varepsilon_{r\infty} + \frac{\varepsilon_{r_S} - \varepsilon_{r\infty}}{1 + (j\omega\tau)^{1-\alpha}} \tag{22}$$

where ε_{r_S} is the relative static permittivity, $\varepsilon_{r\infty}$ is the permittivity for optical frequencies, τ is the relaxation time (i.e. the time it takes for 1/e of the constituent molecules to become aligned in response to an electric field) and alpha is equal to zero for the Debye model whilst is different from zero for the so-called Cole-Cole model.

Another model that can be used in order to fit the results is the Lorentz model. The polarizabilities of Lorentz materials have pairs of complex poles and these materials may exhibit resonant absorption. The relative permittivity of a Lorentz material can be expressed as:

$$\varepsilon_r(\omega) = \varepsilon_{r\infty} + \sum_{n=1}^{N} \frac{A_n \cdot \omega_n^2}{\omega_n^2 + j\omega\gamma_n - \omega^2} \tag{23}$$

where $\varepsilon_{r\infty} = \varepsilon_r^{'} + \dfrac{\sigma}{j\omega\varepsilon_0}$, A_n is the n-th amplitude, ω_n is the n-th Lorentz frequency of a dispersive material, γ_n is the damping frequency and σ the conductivity.

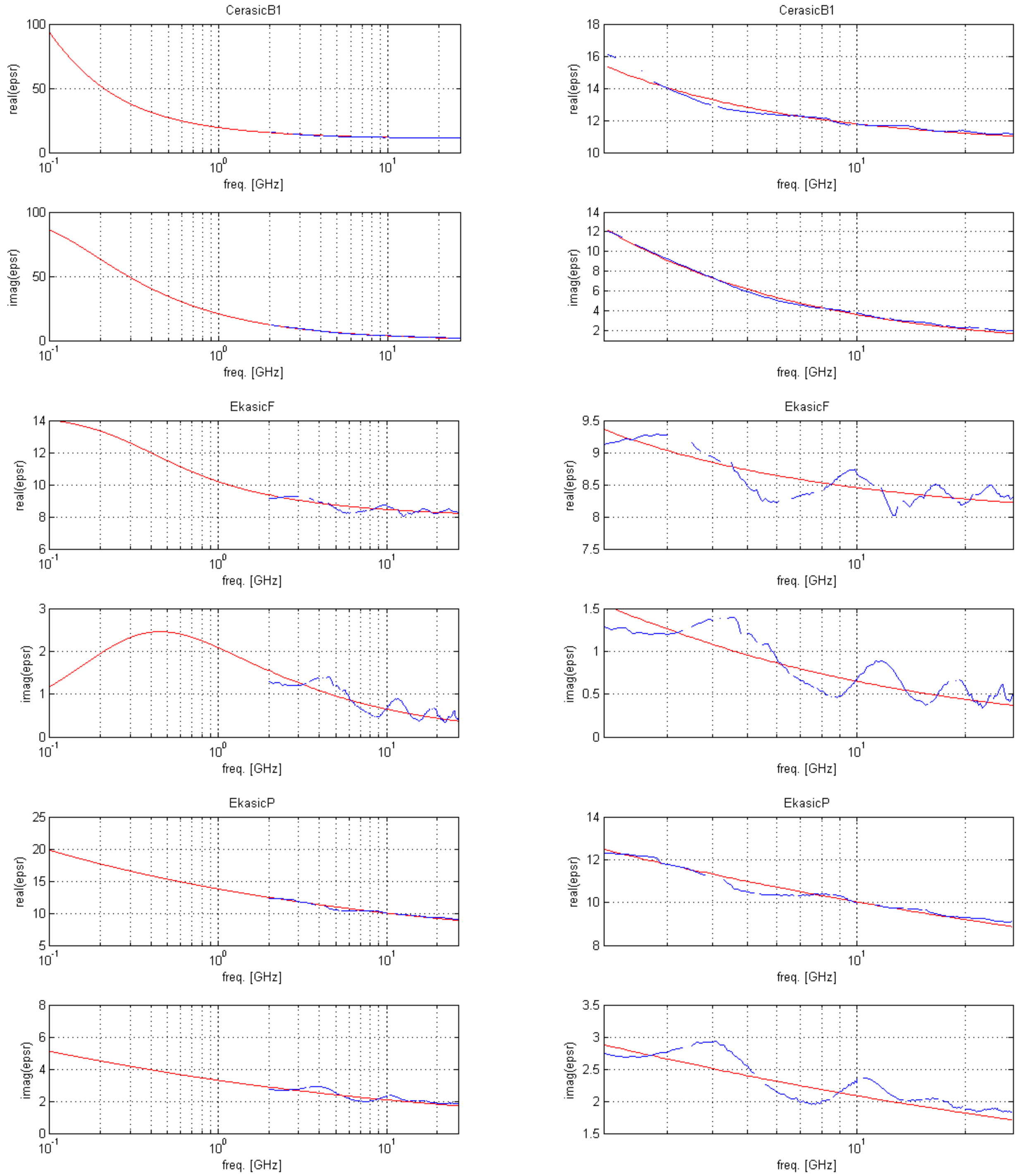

Figure 26: Measurements of permittivity for CerasicB1, EkasicF, EkasicP in the frequency range 2-

27GHz. The measurements are fitted with the Cole-Cole model. The right plots are zoom in the frequency range 2-27GHz.

In general the conductivity can be expressed with the Drude model:

$$\sigma(\omega) = \frac{\sigma_0}{1 + j\omega\tau} \tag{24}$$

where σ_0 is the DC conductivity.

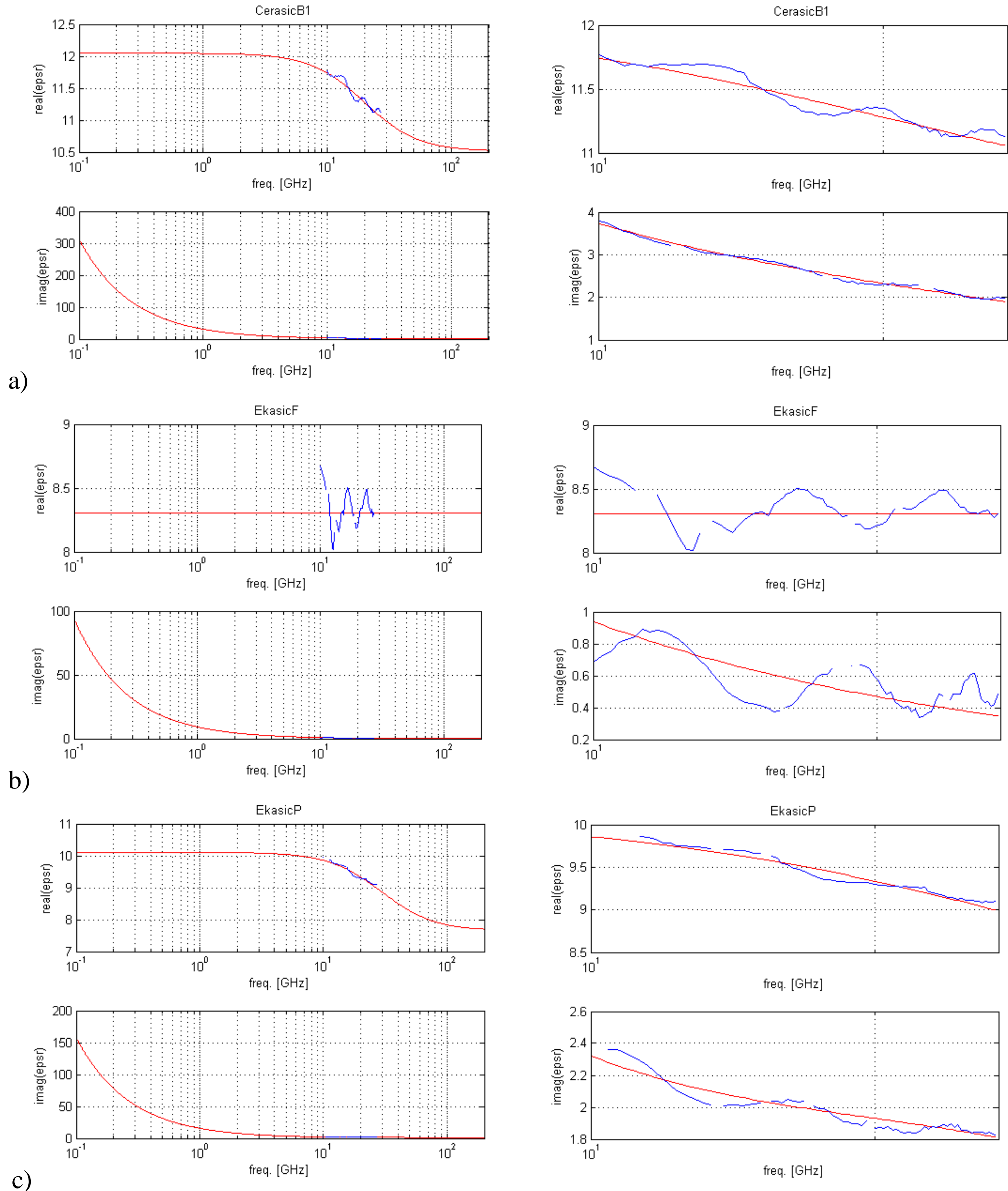

Figure 27: Measurements of permittivity for CerasicB1, EkasicF, EkasicP in the frequency range 10-27GHz. The measurements are fitted with the Lorentz model. The right plots are zoom in the frequency range 10-27GHz.

In order to upload the data in our 3D EM code (GdfidL), we needed to fit the data with a Lorentz model that can be implemented in the solver. Figure 27 shows the fit with the Lorentz model. Figure 28 shows the Cole-Cole plots for the measured materials.

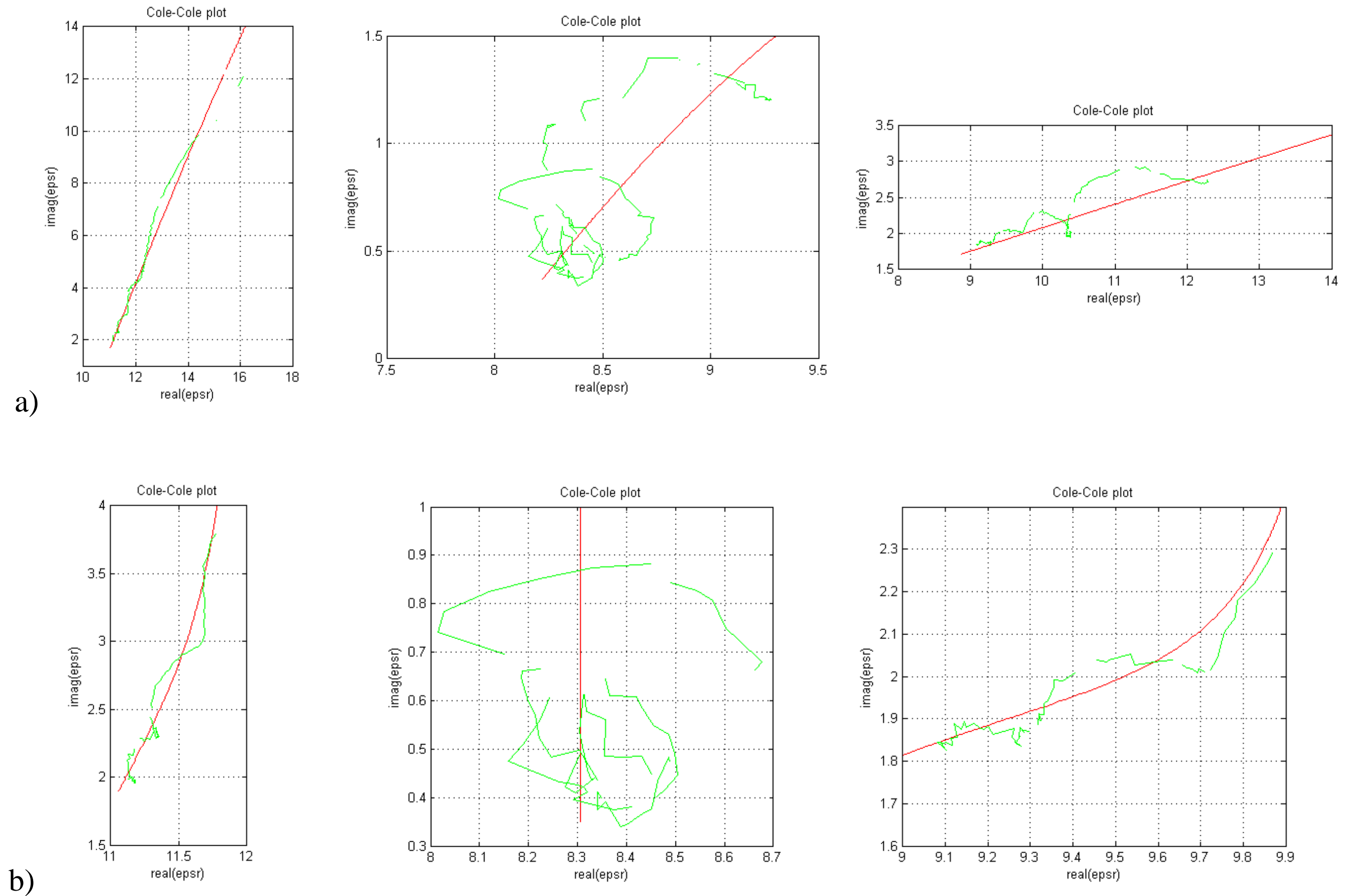

Figure 28: a) Cole-Cole plots (left: CerasicB1, middle: EkasicF, right: EkasicP) for the Cole-Cole model fit, b) Cole-Cole plots (left: CerasicB1, middle: EkasicF, right: EkasicP) for the Lorentz model fit.

d. Error Analysis

Different measurements were performed on the same sample by dismounting and mounting the measurement setup. Figure 29 shows the measurements of S_{21} for EkasicP in the frequency range 2-10 GHz.

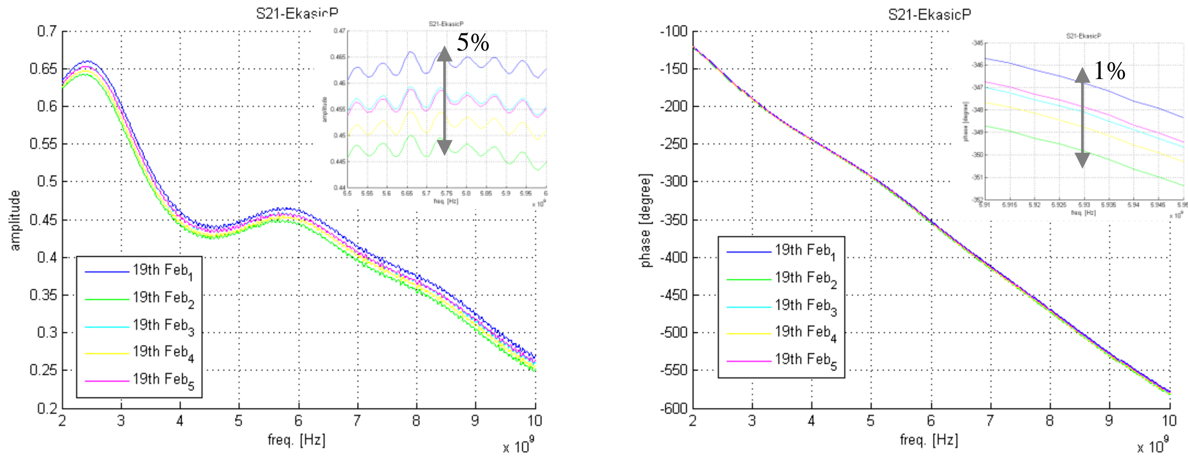

Figure 29: Scattering parameter S_{21} in amplitude and phase for five different measurements on the same sample.

The amplitude of S_{21} shows a total error of 5% whilst the phase of S_{21} only a total error of 1%. This means an error within 5% for the real part of the permittivity and 10% for the imaginary part. Furthermore measurements on different samples for EkasicP in the frequencies ranges: 2-10GHz and 10-27GHz were performed (see Figure 30).

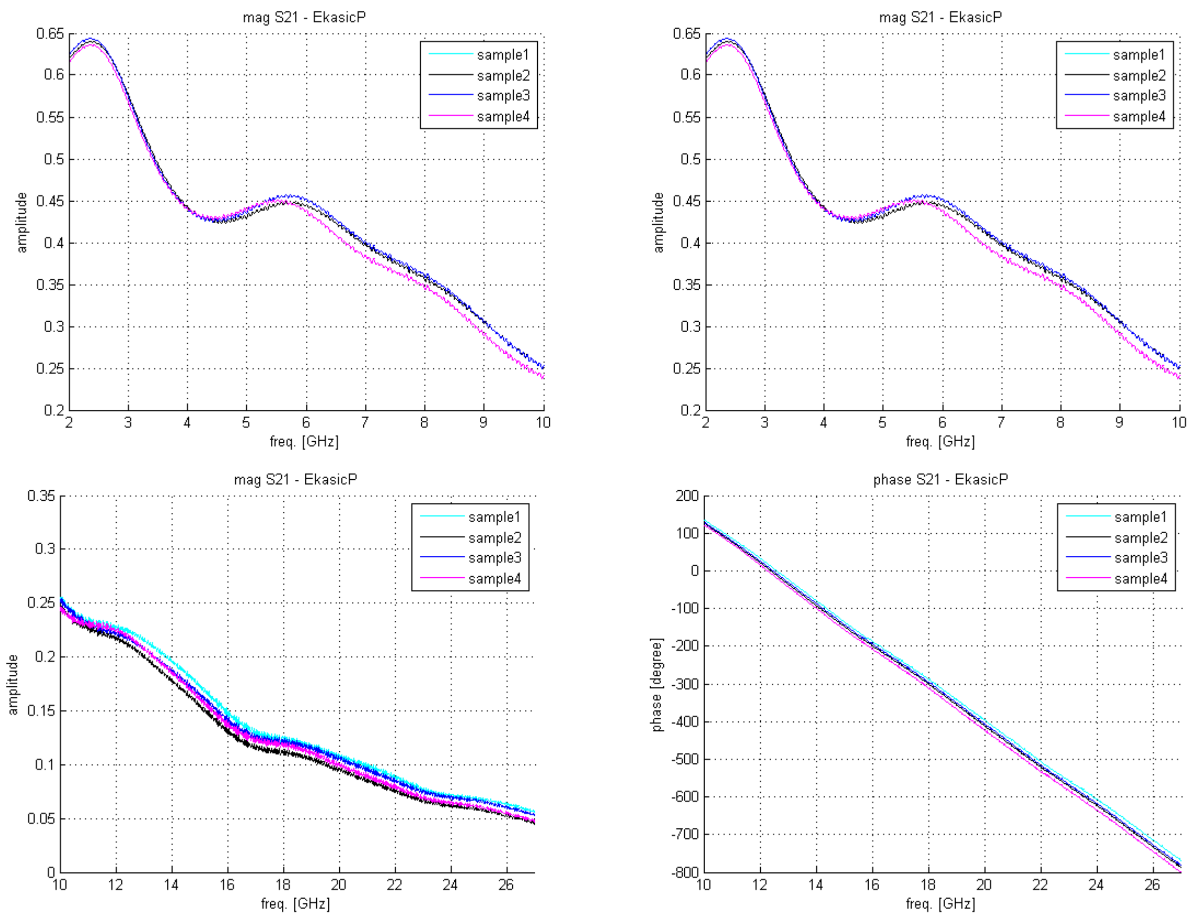

Figure 30: Scattering parameter S_{21} in amplitude and phase for four different samples.

The magnitude and phase variation of S_{21} is within 5% for the frequency range 2-10GHz. This gives a maximum variation of 6% for the real part of permittivity and 9% for imaginary part. The magnitude and phase variation of S_{21} is within 10% and 6% respectively for the frequency range 10-27GHz. This gives a maximum variation of 6% for the real part of permittivity and 9% for imaginary part. Moreover three different calibrations and measurements of EkasicP were performed in the frequency range 2-10GHz (see Figure 31).

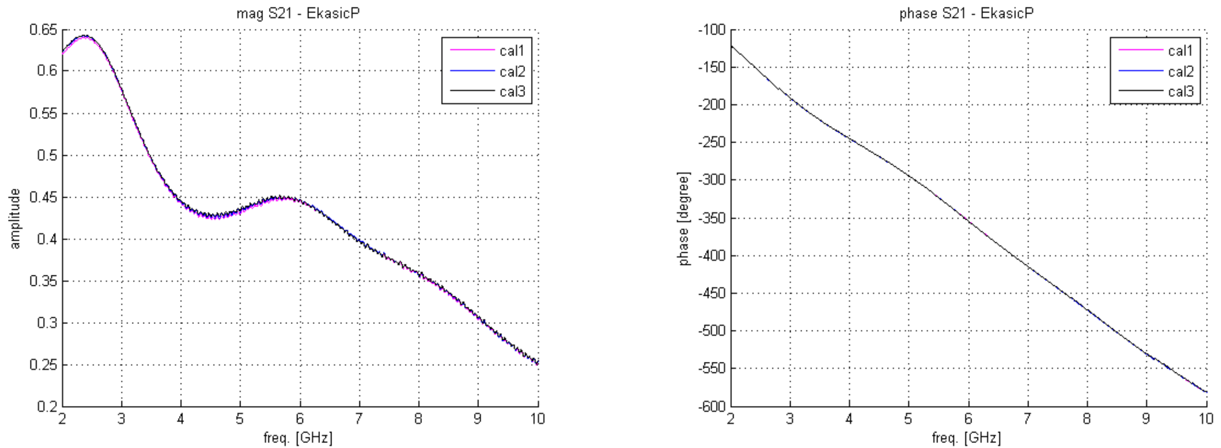

Figure 31: Scattering parameter S_{21} in amplitude and phase for three repeated calibrations.

The magnitude and phase variation of S_{21} is within 1%. This gives a maximum variation of 1% for the real part of permittivity and 2% for imaginary part.

CONCLUSION AND OUTLOOK

The coaxial setup with its simple set-up and transmission line modeling has been used to characterize dielectric materials. Before starting measurements the feasibility of the method was demonstrated in virtual environment (see Figure 5). The results have been presented in a wide range of frequencies for CerasicB1, EkasicF and EkasicP (see Figure 26 and Figure 27).
One of the advantages with respect to the other setups is its wide range of applicability in terms of frequency. The air-gap between the sample and the inner conductor due to machining limitations has been taken into account not only in 3D EM simulations but also in the TL model.
The reflection and the transmission methods have been analyzed and their performance and outcome have been shown.

ACKNOWLEDGEMENTS

One of the authors (G.D.M.) would like to thank C. Zannini for the collaboration work done on the reflection method [7]. His contribution is reported also in his EPFL Ph.D. thesis 2013. G. D. M. would like to thank Prof. V. G. Vaccaro for the discussions and suggestions all along this work. The authors thank G. Riddone and M. Filippova for providing the precise-machining samples. This work was supported by the Swiss National Science Foundation.

REFERENCES

[1] Rohde and Schwarz, *Measurement of Dielectric Material Properties*, Application Note 2006
[2] J. Baker-Jarvis et al., *Improved Techniques for determining Complex Permittivity with the Transmission/Reflection Method*, IEEE Trans. Microwave Th. and Tech., Vol 38, No. 8, August 1990.
[3] A. M. Nicolson and G.F. Ross, *Measurements of the Intrinsic Properties of Materials by Time Domain Techniques*, IEEE Trans. Instrum. Meas., vol IM-17, 1968
[4] M. D. Belrhiti et al., *Complex Permittivity Measurements for Dielectric Materials at Microwave Frequencies using Rectanglar Waveguide*, European Journal of Scientific Research, Vol. 49, No. 2, pp. 234-248, 2011
[5] J. Baker-Jarvis, *Transmission/Reflection and Short-Circuit Line Permittivity Measurements*, National Institute of Standards and Technology, July 1990
[6] R. Fandos, W. Wuensch, *Estimation of the RF Characteristics of Absorbing Materials in Broad RF Frequency Ranges*, CERN-OPEN-2008-019, CLIC-Note-766, 2008.
[7] G. De Michele et al., *Broadband electromagnetic characterization of materials for accelerator components*, IPAC2011, San Sebastián, Spain
[8] G. Fehlen, *Air gap error compensation for coaxial transmission line method of electromagnetic material charachterization*, Air Force Institute of technology, 2006.
[9] http://www.ansys.com